Pergamon

PII: S1352-2310(97)00291-4

Atmospheric Environment Vol. 32, No. 2, pp. 203–214, 1998

1352-2310/98 $17.00 + 0.00

PARTICLE TRAJECTORY SIMULATION OF DISPERSION AROUND A BUILDING

GIOVANNI LEUZZI* and PAOLO MONTI

Dipartimento di Meccanica e Aeronautica, Università degli Studi di Roma "La Sapienza", Via Eudossiana 18, 00184 - Roma, Italia

(*First received* 22 *July* 1996 *and in final form* 17 *June* 1997. *Published November* 1997)

Abstract—Lagrangian stochastic (LS) models have shown to be a powerful technique to calculate pollutant dispersion in complex flows. In this work, a three-dimensional LS model of dispersion has been tested by means of a comparison with EPA wind-tunnel observations of a buoyant plume in the vicinity of a building (Snyder, 1992, *FMF Internal Report*, U.S. Environmental Protection Agency, Research Triangle Park, North Carolina). The model is based on the well-mixed criterion (Thomson, 1987, *Journal of Fluid Mechanics* **180**, 529–556) and is able to evaluate dispersion in inhomogeneous, skew turbulence. The input flow field around the building has been carried out by handling EPA data (Snyder and Lawson, 1993, *FMF Internal Report*, U.S. Environmental Protection Agency, Research Triangle Park, North Carolina). The concentration field predicted by the present model and Thomson's (1987) model have been compared with EPA observations in the same configuration. The dispersion of a tracer emitted from a line source, located at ground level upwind and downwind of the building, has also been investigated, showing the effects of the vortex structure on the mean concentration field. © 1997 Elsevier Science Ltd.

Key word index: Lagrangian stochastic model, atmospheric dispersion, dispersion around a building.

1. INTRODUCTION

Pollutant dispersion in the atmosphere can be successfully predicted by means of Lagrangian stochastic (LS) models. In particular, they are well suited to simulate short-range dispersion in a complex terrain, where strong turbulence inhomogeneities and velocity correlation effects disable eddy-diffusivity techniques.

Up to now, several applications have been performed on complex two-dimensional orography (e.g., Thomson, 1986; Anfossi *et al.*, 1992; Cenedese *et al.*, 1994; Tinarelli *et al.*, 1994; Lanzani and Tamponi, 1995). These models are based on Thomson's (1984, 1986) algorithms. To the authors' knowledge only Näslund *et al.* (1994) applied their LS model in the case of a three-dimensional obstacle. They developed a model which satisfies the well-mixed condition (Thomson, 1987) in the case of Gaussian turbulence. Monti and Leuzzi (1996) implemented a three-dimensional LS model founded on the same condition, but also valid for skew turbulence. They tested the model by comparing numerical results with theoretical predictions (asymptotic behaviour) and with existing wind tunnel observations on flat terrain (Snyder, 1992).

The aims of this paper are to verify the model in the case of dispersion around a three-dimensional building and to investigate the interaction between line source and building. In the next section a brief description of the model equation is reported. Further details on the analytical relationships are given in the appendix. Sections 3 and 4 deal with some aspects regarding the experimental set-up (Snyder, 1992; Snyder and Lawson 1993), and the procedures utilised to derive the model input data from the measurements. A comparison among numerical predictions of our model, Thomson's (1987) model and observations is presented in Section 5. A discussion on the effects of the interaction between line source and building is contained in Section 6.

2. MODEL EQUATIONS

The Lagrangian methods allow the trajectory of particles emitted from a source in a turbulent flow to be followed. The ensemble of the trajectories provides the PDF of particle positions and velocities, from which the mean concentration field can be obtained.

* Author to whom correspondence should be addressed.

In our model each trajectory is evaluated, assuming that the position **x** and the velocity **u** evolve jointly as a Markov process, by the stochastic differential equation system (Thomson, 1987):

$$\begin{aligned} \mathrm{d}u_i &= a_i(\mathbf{x},\mathbf{u},t)\,\mathrm{d}t + b_{ij}(\mathbf{x},\mathbf{u},t)\,\mathrm{d}\xi_j \\ \mathrm{d}x_i &= u_i\,\mathrm{d}t. \end{aligned} \tag{1}$$

The functions a_i and b_{ij} are obtained to guarantee consistency with the flow field, while $\mathrm{d}\xi_j$ are random Gaussian increments with mean zero and variance $\mathrm{d}t$. Values of the increments occurring at different times or in different directions are independent.

According to Thomson (1987), a_i has been evaluated by imposing the well-mixed criterion, i.e., if the particles of tracer are initially well-mixed with respect to both position and velocity, they remain so. By means of this condition and of the Fokker–Plank equation applied to equation (1), a_i takes the form

$$a_i = \frac{1}{2p_a}\frac{\partial}{\partial u_j}(b_{ik}\,b_{jk}\,p_a) + \frac{\phi_i(\mathbf{x},\mathbf{u},t)}{p_a} \tag{2}$$

where p_a is the PDF of the air, which has constant density. The function ϕ_i has to satisfy

$$\frac{\partial \phi_i}{\partial u_i} = -\frac{\partial p_a}{\partial t} - \frac{\partial}{\partial x_i}(u_i p_a)\,, \tag{3}$$

with the constraint $\phi \to 0$ as $|\mathbf{u}| \to \infty$.

In the multi-dimensional case the well-mixed criterion does not provide a unique solution (Sawford and Guest, 1988). The three-dimensional problem has been solved by Thomson (1987) for Gaussian, inhomogeneous turbulence. For skew turbulence a solution has been proposed by Monti and Leuzzi (1996), generalising to three-dimensions the two-dimensional solution proposed by Flesch and Wilson (1992).

The velocities (u,v,w) in a rectangular coordinate system can be transformed to spherical coordinates (s, θ, λ) by means of the following relations:

$$s = \sqrt{u^2 + v^2 + w^2} \quad \theta = \cos^{-1}(w/s) \quad \lambda = \tan^{-1}(v/u). \tag{4}$$

According to Flesch and Wilson (1992), parallelism between $\boldsymbol{\phi}$ and **u** has been assumed (i.e. $\boldsymbol{\phi}$ acts to maintain the **u** direction). This choice is suggested from mathematical convenience rather than physical reasons. Nevertheless, it does not seem to restrict the general validity of the proposed model, as showed by comparisons obtained with different formulations of $\boldsymbol{\phi}$ (Flesch and Wilson, 1992; Monti and Leuzzi, 1996; present paper, Section 5). With the above assumption, ϕ_i becomes

$$\begin{aligned} \phi_u &= \phi_s \sin\theta\cos\lambda \\ \phi_v &= \phi_s \sin\theta\sin\lambda \\ \phi_w &= \phi_s \cos\theta \end{aligned} \tag{5}$$

where ϕ_s, in stationary conditions, assumes the form (Monti and Leuzzi, 1996)

$$\phi_s = -\frac{1}{s^2}\left[\sin\theta\cos\lambda\,\frac{\partial}{\partial x}\int_\infty^s s'^3\,p_a\,\mathrm{d}s' + \sin\theta \times \sin\lambda\,\frac{\partial}{\partial y}\int_\infty^s s'^3\,p_a\,\mathrm{d}s' + \cos\theta\,\frac{\partial}{\partial z}\int_\infty^s s'^3\,p_a\,\mathrm{d}s'\right]. \tag{6}$$

In the numerical simulations the event $s = 0$ never occurs. The computation of the integral $\int_\infty^s s'^3\,p_a\,\mathrm{d}s'$ in equation (6) for Gaussian and non-Gaussian turbulence is described in the appendix.

The function **b** in equation (1) has been evaluated according to the Kolmogorov's theory of local isotropy (Monin and Yaglom, 1975):

$$b_{ik}\,b_{jk} = \delta_{ij}\,C_0\,\varepsilon \tag{7}$$

where ε is the dissipation rate of turbulent kinetic energy and C_0 is a universal constant.

In the numerical simulation a buoyant plume has been considered, therefore a vertical velocity w_b, which takes into account this phenomenon, has to be added to the particle velocity. In the past, the buoyant plume has been frequently treated by the "$\frac{2}{3}$ law" (Briggs, 1975). With reference to the LS model, the plume rise contribution to each particle trajectory can be expressed by

$$H(t) = 1.6\,F_0^{1/3}\,u_s^{-1}\,1\,x_d(t)^{2/3}, \tag{8}$$

where $x_d(t)$ is the downwind distance of a particle from the source, u_s is the mean wind speed at the stack height z_s and $F_0 = g w_s r_s^2\,(T_p - T_e)/T_p$ is the initial buoyancy flux. T_p and T_e are, respectively, the initial plume and the environmental temperatures, w_s is the initial vertical exit speed and r_s is the stack exit radius. However, equation (8) gives incorrect results if the particle velocity u reverses (e.g. in recirculation regions or for strong horizontal turbulence intensity). Consequently, equation (8) has been replaced by the following:

$$H(t) = 1.6\,F_0^{1/3}\,u_s^{-1}\,x_\ell(t)^{2/3} \tag{9}$$

in which $x_\ell(t)$ is the particle path length at the time t. In a finite difference scheme w_b can be evaluated from equations (8) or (9) as follows:

$$w_b = \frac{H(t+\Delta t) - H(t)}{\Delta t}. \tag{10}$$

The $\frac{2}{3}$ law is valid only where the buoyancy effect dominates the ambient turbulence. According to

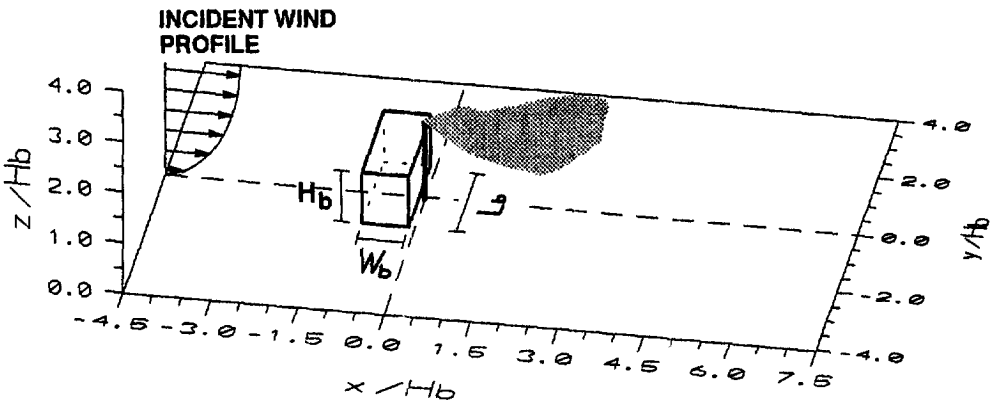

Fig. 1. Schematic representation of the computational domain.

Kranz and Hoult (1973), Anfossi (1982) and Monti and Leuzzi (1996), when w_b becomes less than the local value of the standard deviation of the wind vertical velocity, it is then negligible.

3. SNYDER AND LAWSON EXPERIMENTS

In order to investigate building downwash, the concentration fields in the vicinity of a steam boiler building were measured in the Meteorological Wind Tunnel at the U.S. Environmental Protection Agency (EPA) by Snyder (1992). In the same study, measurements of the velocity and the concentration field were carried out in the absence of the building. The corresponding dispersion phenomenon was numerically investigated by Monti and Leuzzi (1996). In the wind tunnel, a neutral atmospheric boundary layer was simulated, with a depth of 2 m, a roughness length of 1 mm and a scaling ratio of 200:1. The building was a parallelepiped with height $H_b = 250$ mm, width $W_b = 200$ mm and length $L_b = 500$ mm, placed with its long side perpendicular to the mean wind direction (Fig. 1). The associated stack has a height $z_s = 375$ mm and a radius $r_s = 15$ mm.

Mean and variance of the velocities were measured by hot-wire anemometer in the absence of the building. The effluent was a mixture of air, helium and ethane. The buoyancy due to the helium component simulated that due to the higher temperature of the simulated release. A flame ionisation detector measured the concentration of ethane in various sampling port locations.

A detailed study of the full three-dimensional velocity field in the neighbourhood of the building was made by Snyder and Lawson (1993). The simulated boundary layer and the model building were the same as those of the previous study. In this case, a pulsed-wire anemometer was used to measure mean, variance, skewness and kurtosis of the velocities.

4. INPUT DATA

In the Snyder and Lawson experiments (1993), all three velocity components at approximately 2000 unevenly spaced points were measured, in order to provide high resolution where the greatest gradients occur. In the present work, the computational domain lies in the range $-4.5 \leqslant x/H_b \leqslant 7.5$, $-4 \leqslant y/H_b \leqslant 4$, $0 \leqslant z/H_b \leqslant 4$ (Fig. 1) and is subdivided into $60 \times 40 \times 20$ regular grid cells. A linear interpolation in each grid cell has been made. In addition, in order to reduce the divergence of the interpolated mean velocities $(\bar{u}_i, \bar{v}_i, \bar{w}_i)$, the following function:

$$F(\bar{u}, \bar{v}, \bar{w}, \lambda) = \int_V [(\bar{u} - \bar{u}_i)^2 + (\bar{v} - \bar{v}_i)^2 + (\bar{w} - \bar{w}_i)^2 + \lambda \nabla \cdot \bar{u}] \, dx \, dy \, dz \qquad (11)$$

has been minimised according to Sherman (1978). In equation (11), $\bar{u}$, $\bar{v}$ and $\bar{w}$ are the adjusted velocity components and λ is the Lagrangian multiplier. The adjusted velocity vectors in the horizontal plane close to the ground ($z/H_b = 0.1$) are shown in Fig. 2a, and those in the vertical plane along the centreline are shown in Fig. 2b. The length of the recirculating region behind the building is $2.9 H_b$ and its height is $1.2 H_b$. A schematic representation of the main vortices is shown in Fig. 3. The horseshoe vortex forms because of the interaction between oncoming flow and upwind face of the building. Successively it bends along the mean wind direction. The flow separates at the upwind edges, producing separation zones on the roof top and on the sides of the building. Generally, the reattachments occur at the same walls. At the downwind edges the flow separates again, producing the cavity region with a bow vortex.

The variances of the three velocity components are depicted in Figs 4–6. It can be observed that maximum values of $\overline{u'^2}$ occur close to the sides of the building (Fig. 4a). A secondary maximum occurs just above the roof top (Fig. 4b). The $\overline{v'^2}$ maxima are located at analogous positions. The line of maxima descends towards the inside of the recirculation zone (Fig. 5b). The variance $\overline{w'^2}$ shows a similar behaviour (Figs 6a and b). Estimates of skewness and kurtosis of the turbulent velocity were also obtained by Snyder and Lawson

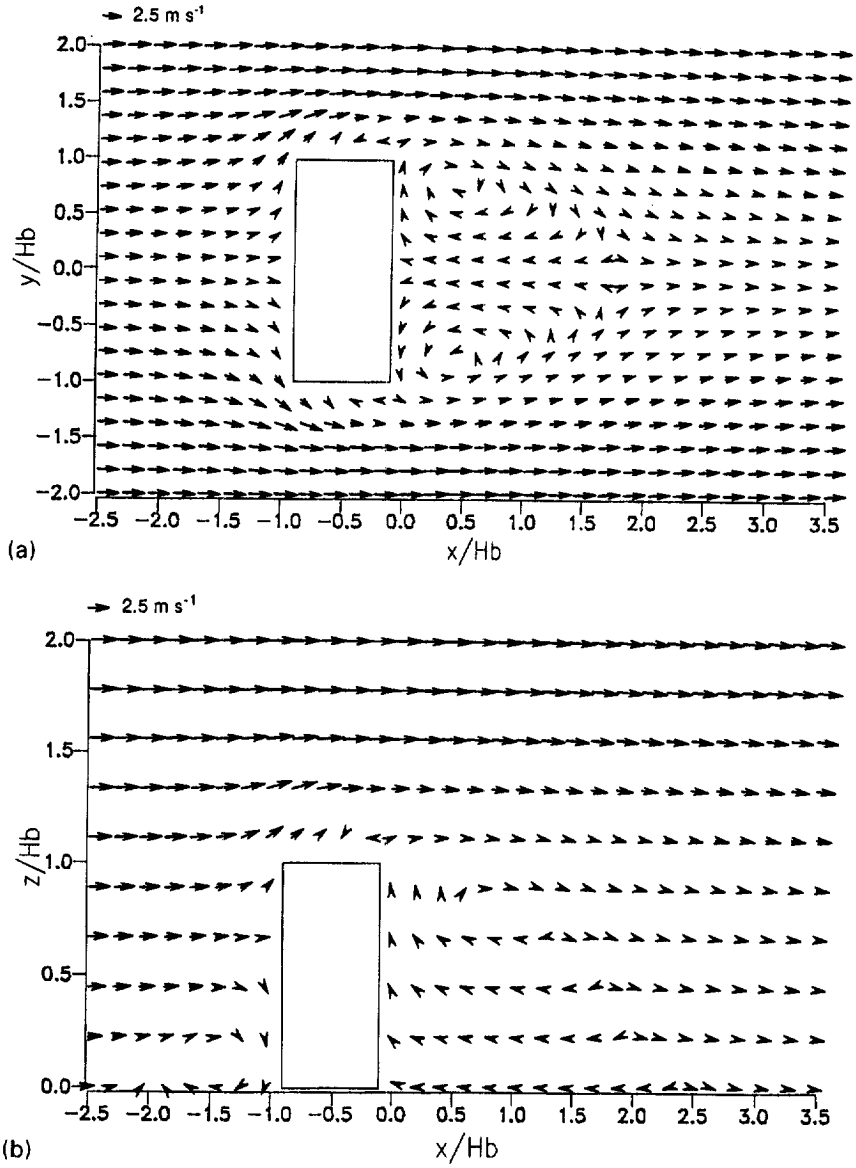

Fig. 2. Adjusted velocity vector field: (a) in the horizontal plane at $z/H_b = 0.1$; (b) in the vertical plane at $y/H_b = 0$.

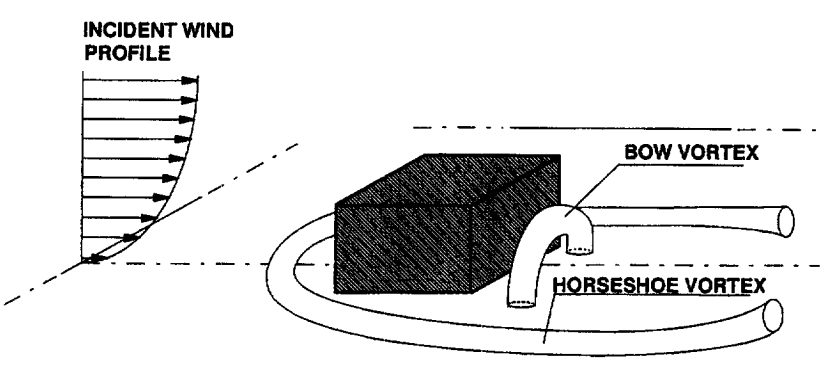

Fig. 3. Schematic representation of the main vortex structures produced by the building.

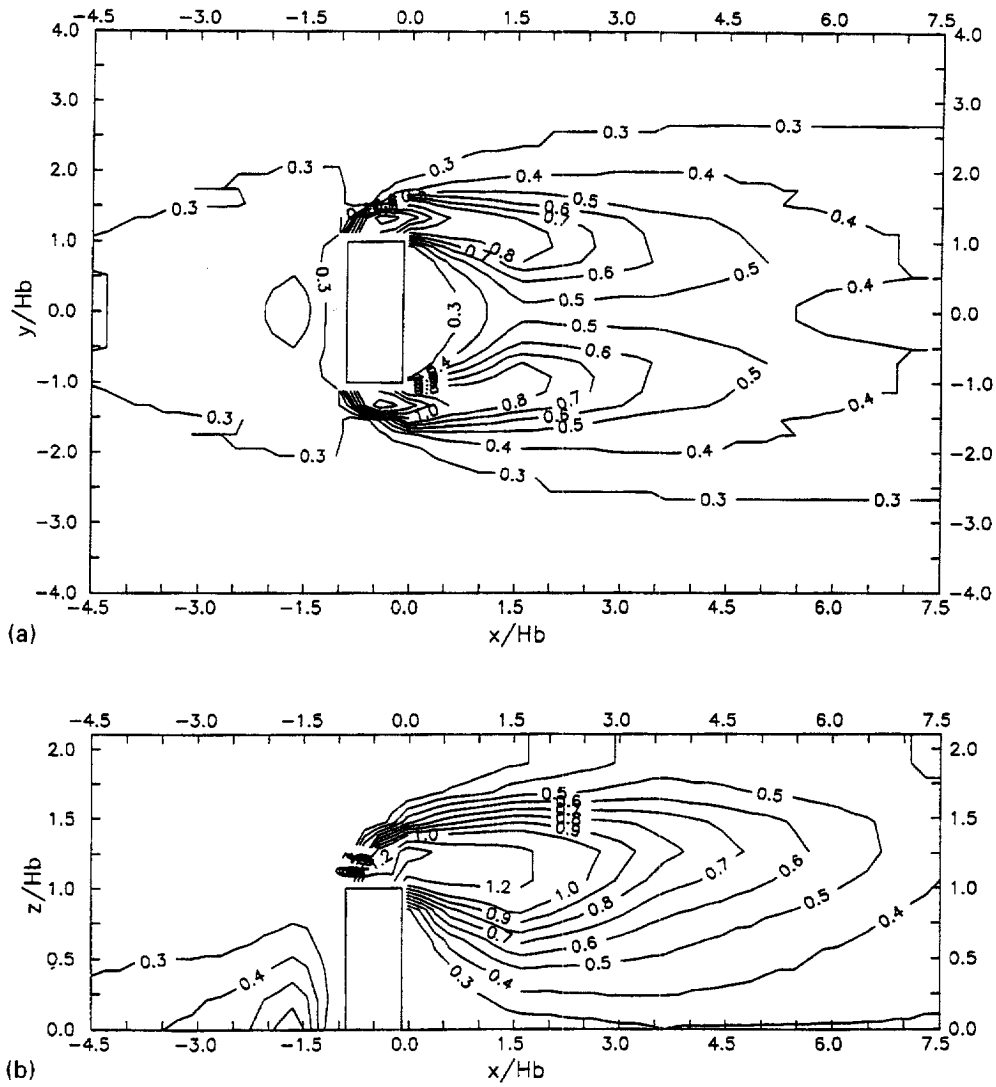

Fig. 4. Variances of the turbulent velocity u, derived from experimental data (Snyder and Lawson, 1993): (a) in the horizontal plane at $z/H_b = 0.1$; (b) in the vertical plane at $y/H_b = 0$.

(1993) but they discourage use of those results, which were strongly dependent on the chosen velocity threshold. As a consequence, in the numerical simulation turbulence has been assumed to be Gaussian. The decorrelation time scale of the turbulence has not been measured. Therefore, τ has been parameterised using the eddy diffusivity of momentum K_m by the following (Berlyand, 1975; Tinarelli *et al.*, 1994):

$$\tau(x,y,z) = \frac{K_m(x,y,z)}{E(x,y,z)} = kC_1^{1/4} \int_0^z \frac{d\zeta}{[E(x,y,\zeta)]^{1/2}} \quad (12)$$

where $k = 0.4$ is the von Karman constant, $E = (\overline{u'^2} + \overline{v'^2} + \overline{w'^2})/2$ is the turbulent kinetic energy and $C_1 = 0.046$. The integral argument in equation (12) has been put to zero inside the building. The time-scale field evaluated by equation (12) is drawn in Figs 7a and b. The building produces a decrement of τ above the roof and within the recirculation region, especially in the vicinity of the maximum variance location ($x/H_b \cong 1.8$).

5. COMPARISON BETWEEN PARTICLE MODELS AND EXPERIMENTS OF SNYDER AND LAWSON

In order to validate our LS model, comparisons between the estimated and experimental concentrations have been performed. A further comparison can be made with the Thomson's (1987) model. In this formulation, a_i is

$$a_i = -\frac{1}{2} b_{ik} b_{jk} (\sigma^{-1})_{jk} (u_k - \bar{u}_k) + \frac{\phi_i}{p_a} \quad (13)$$

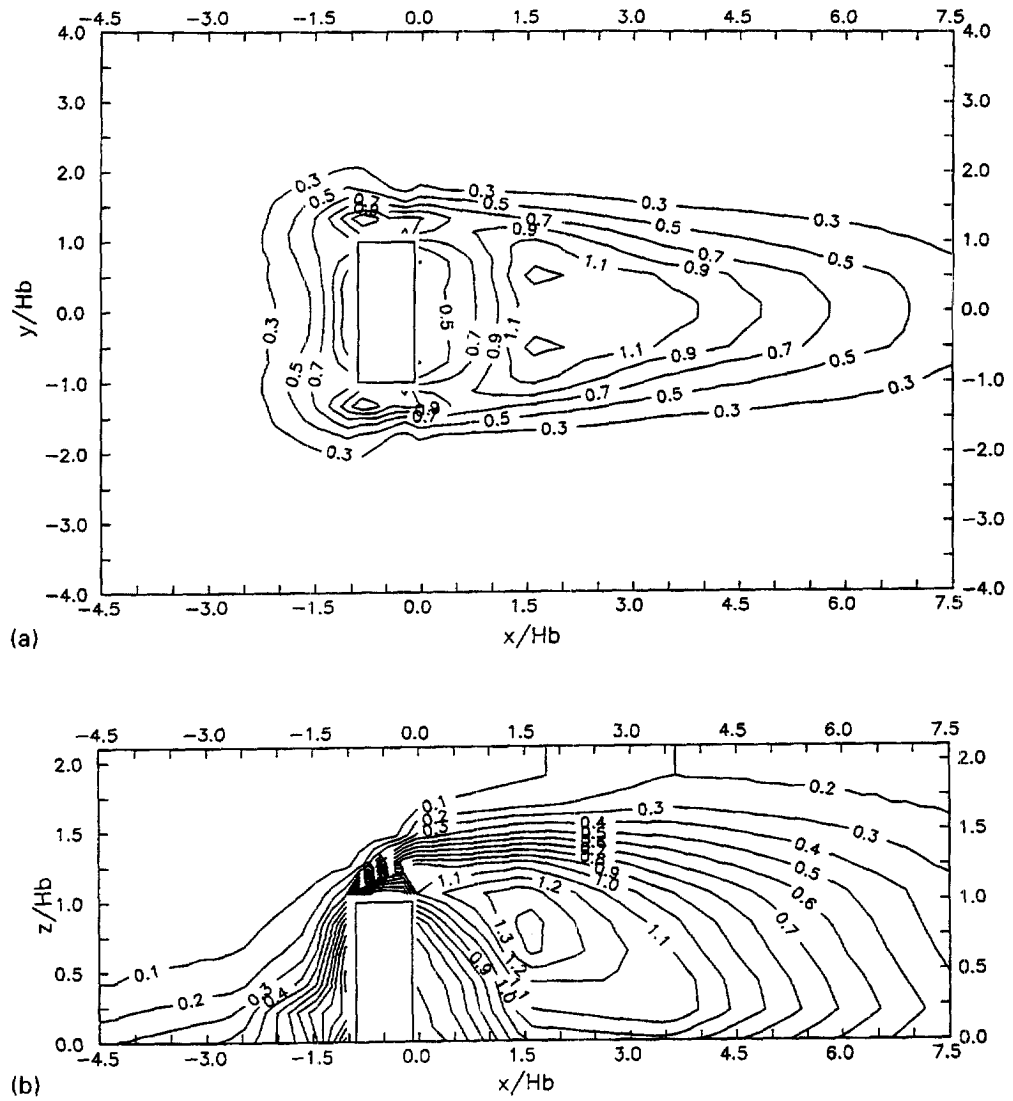

Fig. 5. Variances of the turbulent velocity v, derived from experimental data (Snyder and Lawson, 1993): (a) in the horizontal plane at $z/H_b = 0.1$; (b) in the vertical plane at $y/H_b = 0$.

where $\boldsymbol{\sigma}$ is the covariance matrix and ϕ_i/p_a:

$$\frac{\phi_i}{p_a} = \frac{1}{2}\frac{\partial \sigma_{il}}{\partial x_l} + \bar{u}_l \frac{\partial \bar{u}_i}{\partial x_l} + \left(\frac{1}{2}(\boldsymbol{\sigma}^{-1})_{lj}\left(\bar{u}_m \frac{\partial \sigma_{il}}{\partial x_m}\right) + \frac{\partial \bar{u}_i}{\partial x_j}\right) \times (u_j - \bar{u}_j) + \frac{1}{2}(\boldsymbol{\sigma}^{-1})_{lj}\frac{\partial \sigma_{il}}{\partial x_k}(u_j - \bar{u}_j)(u_k - \bar{u}_k). \quad (14)$$

The concentration measurements were carried out with a free stream velocity ($u_\infty = 1.23\ \mathrm{m\,s^{-1}}$) smaller than that of the velocity field measurements ($u_\infty = 4\ \mathrm{m\,s^{-1}}$). As pointed out by Snyder (1992), the effect of effluent speed to wind speed ratio w_s/u_s is strong in the presence of the building. Thus, in order to maintain this ratio, in the derivation of the simulated buoyancy flux the effluent speed has been increased by the ratio 4/1.23 (w_s becomes equal to $4.615\ \mathrm{m\,s^{-1}}$). All the parameters in the plume-rise equation (9) have been referred to full-scale case values. The length scale was 200:1 and the velocity scale has been obtained to maintain the Froude number $Fr = w_s^2/2gr_s[(T_p - T_e)/T_e] = 16$ of the experiment. For the simulated ratio $(T_p - T_e)/T_e = 0.426$, a velocity scale equal to 4.268 has been evaluated.

In the numerical simulation 2.5×10^4 fictitious particles were emitted from the stack at a height $z_s/H_b = 1.5$ (Fig. 1). Equation (1) has been integrated by a finite difference scheme with a time step $\Delta t = 0.006$ s. A perfect reflection has been assumed at the boundaries (top and bottom of the domain

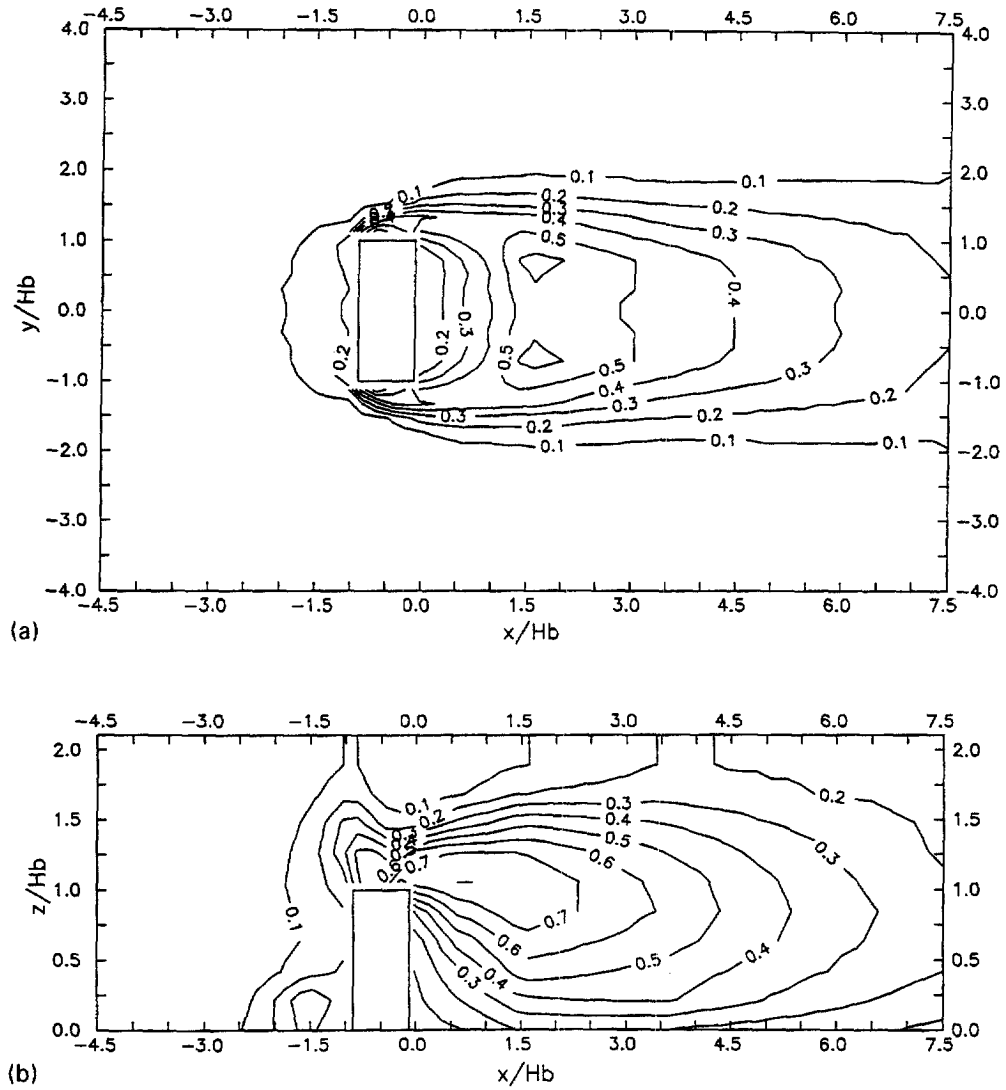

Fig. 6. Variances of the turbulent velocity w, derived from experimental data (Snyder and Lawson, 1993): (a) in the horizontal plane at $z/H_b = 0.1$; (b) in the vertical plane at $y/H_b = 0$.

including the building surfaces). The lowering of the top at $z/H_b = 4$ does not increase the mean concentration within the boundary layer. In fact, for the considered downwind distance, the particles do not reach the assumed top. According to Snyder (1992), computed concentration $\tilde{c}$ was normalised by the approaching flow wind speed at $z = 10$ m and the volumetric flow rate Q, to give $\bar{C} = 10^{-6}\,\tilde{c}u_{10}/Q$. Figure 8 shows the comparison between measured and computed normalised concentration at two downwind distances from the source: 2.5 H_b and 5 H_b. At the first downwind location only the vertical profile of measured concentration was available (Fig. 8a). The general agreement between predicted results and measurements is satisfactory. The peak concentrations and their positions match the observed values, confirming the validity of the models and the buoyancy modelling also in the case of complex flows in recirculation regions. Nevertheless, an overprediction of the concentration appears just above the ground and an underprediction above the height of the maximum. The Thomson's model predicts better the concentration below $z/H_b = 1.2$, but underpredicts the values above. The discrepancy between measurements and predictions could be due to an inaccuracy in the evaluation of τ, to the assumption of Gaussianity of the turbulence or to the absence of observations on velocity covariance. At the second downwind location, both lateral and vertical observed profiles were available (Figs 8b and c). The predicted lateral profiles reproduce quite well the measured values. As for the previous location, in the vertical plane the performance of the models are satisfactory, with the exception of the overestimation at the lower

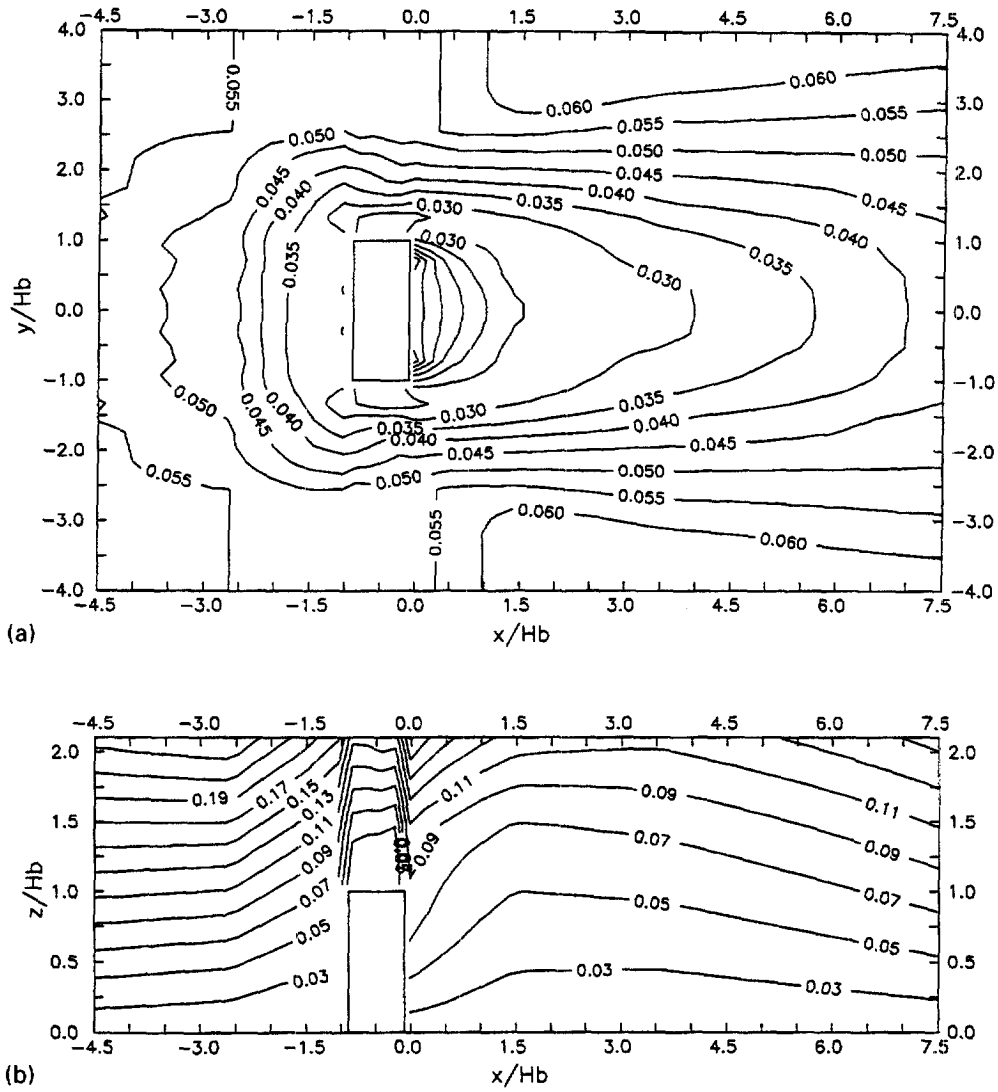

Fig. 7. Decorrelation time scale calculated by equation (12): (a) in the horizontal plane at $z/H_b = 0.1$; (b) in the vertical plane at $y/H_b = 0$.

region. Bearing in mind the unavailability of some input data (e.g. skewness and decorrelation time scale) and the extension of the $\frac{2}{3}$ law in the case of complex flows, the numerical predictions are satisfactory.

The comparisons between the two models show a general insensitivity of the solutions from the assumed formulations of ϕ. In the case of flat terrain an analogous conclusion was drawn by Flesch and Wilson (1992). Finally, we can assert that both the models are suitable to describe dispersion around obstacles, where strong turbulence inhomogeneities and recirculation effects occur. The non-Gaussian nature of the turbulence seems to be not important in the case proposed, but our model is more versatile in view of the application in convective conditions, where it is necessary to take account of the turbulence asymmetry.

6. INTERACTION BETWEEN LINE SOURCE AND BUILDING

In this section, our LS model has been applied in the case of a line source at ground level, upwind and downwind of the building. These are typical configurations in the study of the environmental impact produced by motor vehicle traffic. In this way, for example, it is possible to estimate the concentrations at the intakes of building ventilation systems, or the exposure of pedestrians in the vicinity of the building.

In the numerical simulation the building and the corresponding flow field are the same as those used in the previous section. The line source emits non-reactive and non-buoyant pollutant at a constant rate. In particular, two cases have been considered,

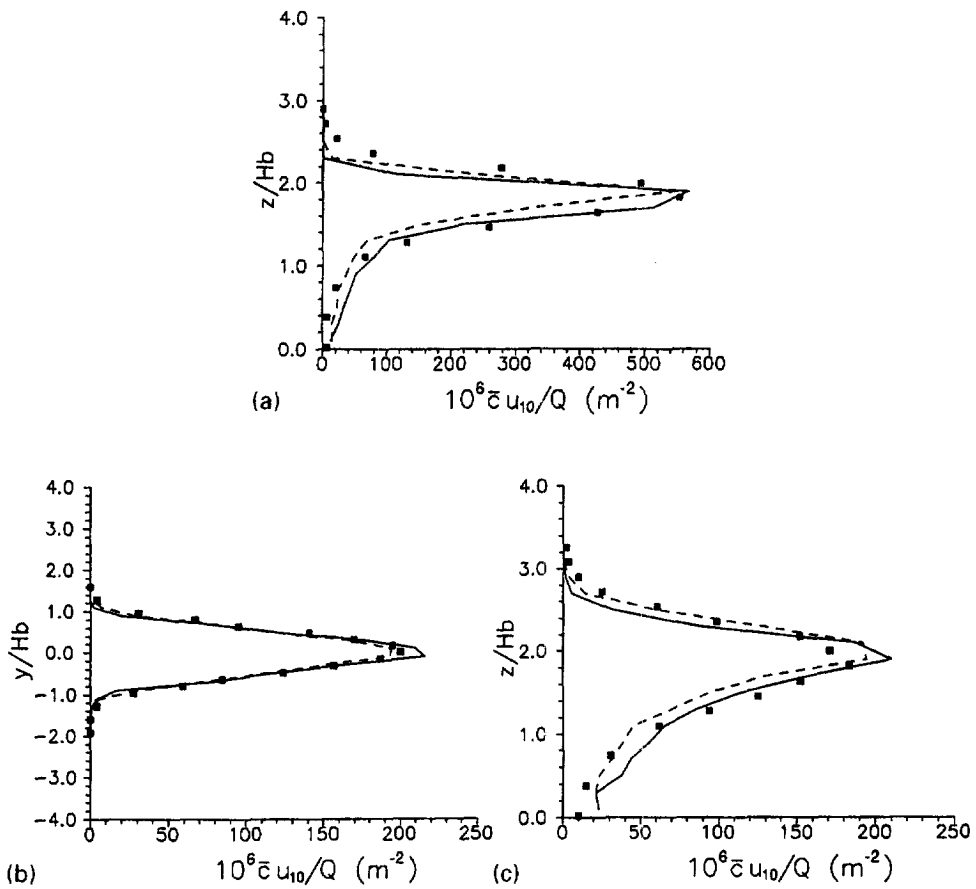

Fig. 8. Comparison between normalised concentration: predicted by our model (continuous line), Thomson's (1987) model (dashed line) and observed by Snyder (1992) (squares): (a) vertical profiles at $x/H_b = 2.5$, $y/H_b = 0$. (b) horizontal profiles at $x/H_b = 5$, $z/H_b = 1.88$. (c) vertical profiles at $x/H_b = 5$, $y/H_b = 0$.

with the source located, respectively, at $x/H_b = -1.06$, $z/H_b = 0.01$ and $x/H_b = -0.06$, $z/H_b = 0.01$.

In Fig. 9 the mean concentration field for the upwind source location is shown. The concentration has been normalised with the value which occurs when the pollutant is homogeneously distributed. Figure 9a shows the results in the horizontal plane ($z/H_b = 0.1$). Pollutant particles collect near the upwind surface of the building, within the horseshoe vortex (see Fig. 3). They remain trapped and are advected downstream. Such behaviour gives rise to high concentration levels which make the vortex structure readily visible. In the lee of the building there is a corresponding deficit, since particles initially outside of the bow vortex cannot readily enter it. As a consequence, low concentrations occur within such a vortex and only a slight amount of particles penetrates into the region just behind the vortex. Figure 9b shows a vertical section of the concentration field along the centreline. On the lee side the pollutant is advected upwards.

The computed concentrations for a source located downwind of the building are shown in Figs 10a and b. The emitted particles stagnate at ground level in the immediate lee of the building, then stay for a long time in the bow vortex, increasing the concentration levels. Also in this case high pollutant concentrations occur at locations corresponding to the horseshoe vortex. A video image analysis of the effects of building geometry and source location on diffusion in building wakes was reported by Lee *et al.* (1991). They observed that for a downwind source the vortex shedding from the corner of the building was very unsteady. The vortices move and shed alternately from each side of the building, inducing time-averaged concentration peaks near each corner, in agreement with our results. Because of the different source geometry (point source instead of line source), in their analysis the effects of the horseshoe vortex were not emphasised.

From a general analysis of the numerical results, we can observe that for wind direction along the x-axis only the building sides are not effected by high

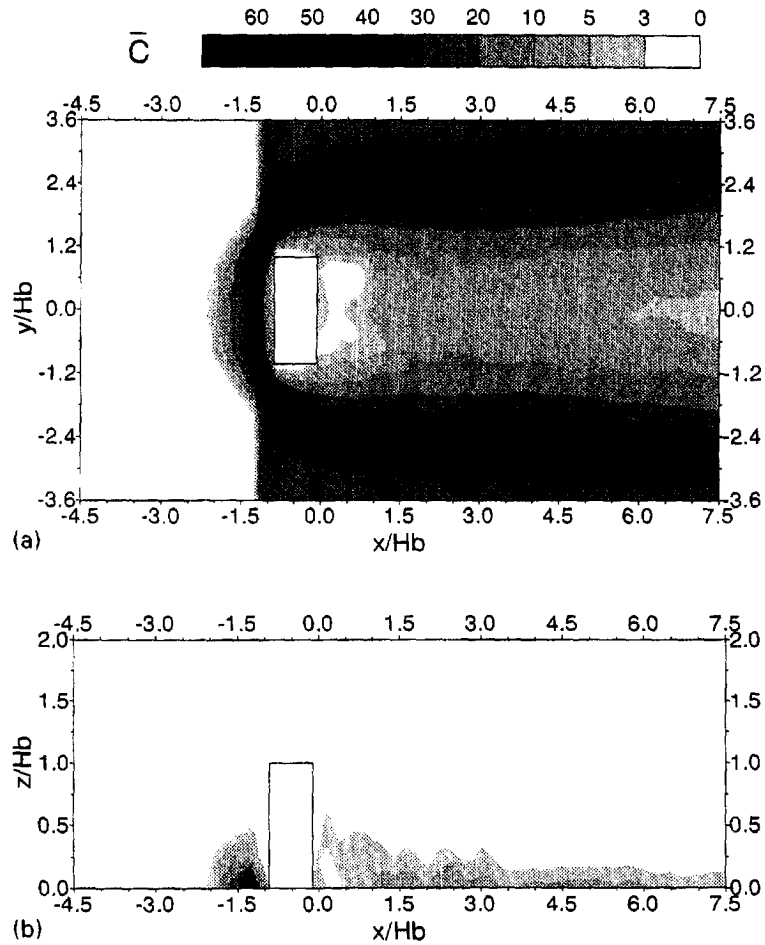

Fig. 9. Maps of the normalised concentration for an upwind line source located at $x/H_b = -1.06$, $z/H_b = 0.01$: (a) horizontal section at $z/H_b = 0.01$. (b) vertical section at $y/H_b = 0$.

concentration levels. In both the considered configurations, the roof top is rarely reached by the particles emitted. However, in practice, there are often further pollutant sources (e.g. chimney-stacks) which strongly increase the concentration levels.

7. CONCLUSIONS

In this paper a three-dimensional, LS model has been tested in the case of dispersion around a building. Although the formulation takes account of the skew turbulence, only Gaussian applications has been presented. The model is based on the well-mixed criterion (Thomson, 1987) and has been developed by the authors in work reported elsewhere (Monti and Leuzzi, 1996). In the present paper the concentrations predicted by our model and Thomson's (1987) model have been compared with the experimental results obtained by Snyder (1992) in the presence of a building, utilising as input data the velocity field obtained from measurements made by Snyder and Lawson (1993) in the same configuration. According to these authors, data on skewness have been discarded for the lack of reliability. To simulate the experimental conditions, a neutral boundary layer and a buoyant plume have been considered.

From a general analysis of the results, we can state that despite the complexities of the flow, the agreement between predictions and observations is qualitatively and quantitatively satisfactory. Lateral spread, peak concentration values and their locations are correctly evaluated, confirming also the validity of the adopted plume-rise scheme. Some discrepancies have been observed near the ground, which might be due to the inaccuracy of the decorrelation time-scale modelling or to the absence of information on skewness and covariance velocity.

Thomson (1987) model is more physically motivated than the present formulation and appears to provide as good results as our model. Nevertheless, our formulation should have a wider application field (e.g. dispersion in convective boundary layer).

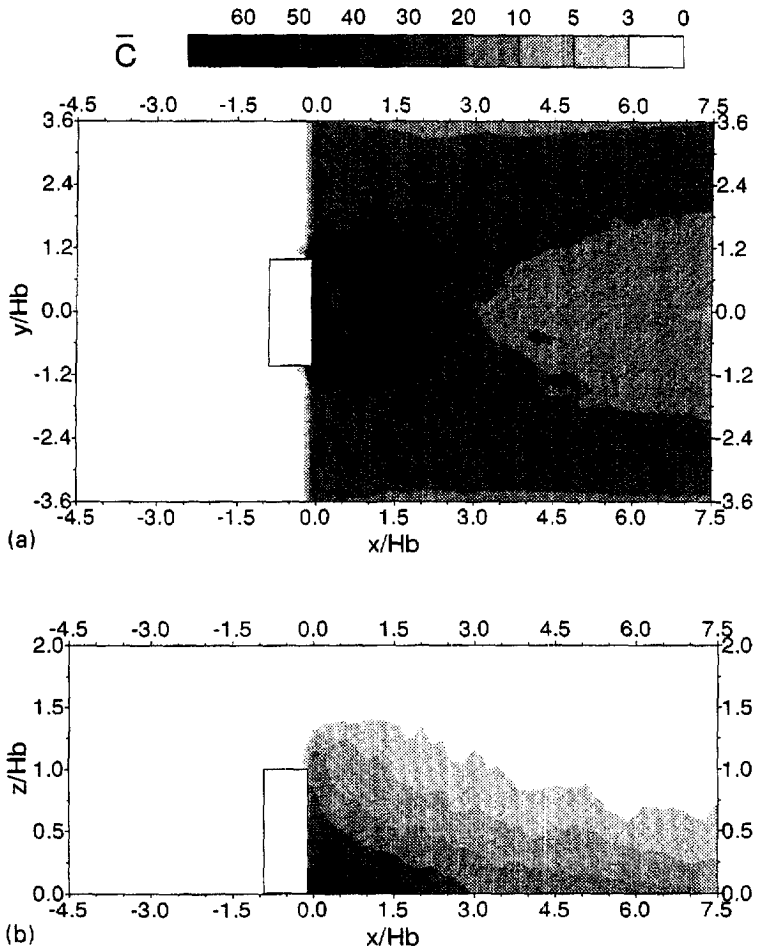

Fig. 10. Maps of the normalised concentration for a downwind line source located at $x/H_b = -0.06$, $z/H_b = 0.01$: (a) horizontal section at $z/H_b = 0.01$. (b) vertical section at $y/H_b = 0$.

A further investigation in the case of line sources, simulating motor vehicle emissions, has been reported. The complex interaction between vortex structures and dispersion phenomenon has been described, and zones with lower pollutant concentration have been identified.

Acknowledgements—The authors would like to thank Prof. W. H. Snyder for supplying the experimental data and Dr. F. Trombetti for bibliographical material.

REFERENCES

Anfossi, D., Ferrero, E., Brusasca, G., Marzorati, A., Tinarelli, G., Tampieri, F., Trombetti F. and Giostra, U. (1992) Dispersion simulation of a wind tunnel experiment with lagrangian particle models. *Il Nuovo Cimento* **15C**, 139–158.

Anfossi, D., Ferrero, E., Brusasca, G., Marzorati, A. and Tinarelli, G. (1993) A simple way of computing buoyant plume rise in lagrangian stochastic dispersion models. *Atmospheric Environment* **27A**, 1443–1451.

Berlyand, M. E. and Genikhovich, E. L. (1971) Atmospheric diffusion and the structure of the air flow above an inhomogeneous surface. *Proceedings of the International Symposium on Meteorological Aspects Air Pollution*, 1968, Leningrad, Hydrometeor Press, pp. 43–69.

Briggs, G. A. (1975) Plume rise prediction. In *Lectures on Air Pollution and Environmental Impact Analysis*. American Meteorological Society, Boston.

Cenedese, A., Leuzzi, G. and Monti, P. (1994) Effects produced by velocity covariance on a Lagrangian model of dispersion over obstacles. In *Stably Stratified Flows: Flow and Dispersion over Topography*, ed. I. P. Castro and N. J. Rockliff, pp. 291–300. Clarendon, Oxford.

Du, S., Wilson, J. D. and Yee, E. (1994) Probability density functions for velocity in the convective boundary layer, and implied trajectory models. *Atmospheric Environment* **28**, 1211–1217.

Flesch, T. K. and Wilson, J. D. (1992) A two-dimensional trajectory-simulation model for non-gaussian, inhomogeneous turbulence within plant canopies. *Boundary-Layer Meteorology* **61**, 349–374.

Kranz, W. T. and Hoult, D. P. (1973) *Design Manual for Tall Stacks*. MIT Publishers Cambridge, MA.

Lanzani, G. and Tamponi, M. (1995) A microscale Lagrangian particle model for the dispersion of primary pollutants in a street canyon sensitivity analysis and first validation trials. *Atmospheric Environment* **29**, 3465–3475.

Lee, J. T., Call, D. L., Lawson, R. E. Jr., Clements, W. E. and Hoard, D. E. (1991) A video image analysis system for concentration measurements and flow visualisation in building wakes. *Atmospheric Environment* **25A**, 1211–1225.

Monin, A. S. and Yaglom, A. M. (1975) *Statistical Fluid Mechanics*, Vol. 2. MIT Press, Cambridge, MA.

Monti, P. and Leuzzi, G. (1996) A closure to derive a three-dimensional well-mixed trajectory model for non-gaussian, inhomogeneous turbulence. *Boundary-Layer Meteorology* **80**, 311–331.

Näslund, E., Rodean, H. C. and Nasstrom, J. S. (1994) A comparison between two stochastic diffusion models in a complex three-dimensional flow. *Boundary-Layer Meteorology* **67**, 369–384.

Sawford, B. L. and Guest, F. M. (1988) Uniqueness and universality of Lagrangian stochastic models of turbulent dispersion. *Proceedings American Meteorological Society, 8th Turbulence and Diffusion Symposium*, 25–29 April, San Diego, pp. 96–99.

Sherman, C. A. (1978) A mass-consistent model for wind fields over complex terrain. *Journal of Applied Meteorology* **17**, 312–319.

Snyder, W. H. (1992) Wind-tunnel simulation of building downwash from electric-power generating stations. Part I: boundary layer and concentration measurements. *Fluid Modeling Facility Internal Report*, Environmental Protection Agency, Research Triangle Park, North Carolina.

Snyder, W. H. and Lawson, R. E. Jr. (1993) Wind-tunnel simulation of building downwash from electric-power generating stations. Part II: pulsed-wire measurements in the vicinity of steam-boiler building. *Fluid Modeling Facility Internal Report*, Environmental Protection Agency, Research Triangle Park, North Carolina.

Thomson, D. J. (1984) A random walk modelling of diffusion in inhomogeneous turbulence. *Quarterly Journal of the Royal Meteorological Society* **110**, 1107–1120.

Thomson, D. J. (1986) A random walk model of dispersion in turbulent flows and its application to dispersion in a valley. *Quarterly Journal of the Royal Meteorological Society* **112**, 511–530.

Thomson, D. J. (1987) Criteria for the selection of stochastic models of particle trajectories in turbulent flows. *Journal of the Fluid Mechanics* **180**, 529–556.

Tinarelli, G., Anfossi, D., Brusasca, G., Ferrero, E., Giostra, U., Morselli, M. G., Moussafir, J., Tampieri, F. and Trombetti, F. (1994) Lagrangian particle simulation of tracer dispersion in the lee of a schematic two-dimensional hill. *Journal of Applied Meteorology* **33**, 744–756.

APPENDIX

In the case of Gaussian turbulence, p_a takes the form:

$$p_a = \frac{1}{(2\pi)^{3/2}(\det\ \boldsymbol{\sigma})^{1/2}} \exp\left[-\frac{1}{2}(u_i - \bar{u}_i)(\boldsymbol{\sigma}^{-1})_{ij}(u_j - \bar{u}_j)\right] \tag{A1}$$

where $\boldsymbol{\sigma}$ is the covariance matrix and $\bar{u}$ is the mean velocity vector. In spherical coordinates p_a becomes:

$$p_a(\mathbf{x}, s, \theta, \lambda) = \frac{1}{(2\pi)^{3/2}(\det\ \boldsymbol{\sigma})^{1/2}} \exp\left[-\tfrac{1}{2}(A_2 s^2 + A_1 s + A_0)\right] \tag{A2}$$

where:

$$A_0 = \tfrac{1}{2}\sigma_{ij}\bar{u}_i\bar{u}_j$$

$$A_1 = -\sigma_{1i}\bar{u}_i\cos\lambda\sin\theta - \sigma_{2i}\bar{u}_i\sin\lambda\sin\theta - \sigma_{3i}\bar{u}_i\cos\theta \tag{A3}$$

$$A_2 = \tfrac{1}{2}(\sigma_{11}\cos^2\lambda\sin^2\theta + \sigma_{22}\sin^2\lambda\sin^2\theta + \sigma_{33}\cos^2\theta) + \sigma_{12}\cos\lambda\sin\lambda\sin^2\theta + \sigma_{23}\cos\theta\sin\lambda\sin\theta + \sigma_{13}\cos\lambda\cos\theta\sin\theta.$$

Thus, the integral in equation (6) yields:

$$\int_{\infty}^{s} s'^3 p_a\, ds' = \frac{1}{(2\pi)^{3/2}(\det\boldsymbol{\sigma})}\left\{\frac{-4A_2^2 s^2 + 2A_2A_1 s - 4A_2 - A_1^2}{8A_2^3} \times \exp\left[-(A_2 s^2 + A_1 s + A_0)\right] + \frac{-(\pi)^{1/2}(6A_1A_2 + A_1^3)\exp\left(\frac{A_1^2}{4A_2} - A_0\right)}{16A_2^{7/2}} \times\left[\mathrm{Erf}\left(\frac{A_1 + 2A_2 s}{2(A_2)^{1/2}}\right) - 1\right]\right\}. \tag{A4}$$

The extension to non-Gaussian turbulence has been carried out by considering a linear combination of eight Gaussian PDFs:

$$p_a = \alpha_1^{(l)}\alpha_2^{(m)}\alpha_3^{(n)} g^{(lmn)} \quad l = 1,2, \quad m = 1,2, \quad n = 1,2, \tag{A5}$$

in which $\alpha_p^{(q)}$ are coefficients to determine and $g^{(lmn)}$ is a trivariate Gaussian PDF with means $m_1^{(l)}$, $m_2^{(m)}$, $m_3^{(n)}$ and standard deviations $r_1^{(l)}$, $r_2^{(m)}$, $r_3^{(n)}$ in the directions 1, 2 and 3, respectively. The correlation coefficient ρ_{ij} has been assumed the same for all the eight Gaussian PDF. All the above unknowns can be determined by equating the first four moments obtained from the right-hand side in equation (A5) to the given moments of the air velocity. An analogous procedure may be adopted for the mixed moments. A detailed description of the solution was made by Scarani (1991) and Monti and Leuzzi (1996). Imposing $r_i^{(1)} = r_i^{(2)}$ for $i = 1,2,3$, the following expressions have been developed:

$$r_i^{(1)} = \beta Sd_i + (1-\beta)\left(2\frac{|Cov_{ij}|}{Sd_j} - \frac{1}{2}\frac{|Cov_{jk}|\,Sd_i}{Sd_j Sd_k}\right) \tag{A6}$$

$$\alpha_i^{(1)} = \frac{\xi_i}{\xi_i + \zeta_i}, \quad \alpha_i^{(2)} = 1 - \alpha_i^{(1)} \tag{A7}$$

$$m_i^{(1)} = M_i - \zeta_i, \quad m_i^{(2)} = M_i + \xi_i \tag{A8}$$

where β is a coefficient lying in the range $(0,1)$, Cov_{ij} is the covariance of air velocity components in i and j directions and M_i and Sd_i are, respectively, mean and standard deviation of air velocity. Denoting the second- and third-dimensional moments by Sq_i and Sk_i, respectively, the terms ξ_i and ζ_i can be obtained by:

$$\xi_i = \frac{\sqrt{\gamma_i^2 + 4(Sq_i - M_i^2)^3} - M_i(3Sq_i - 2M_i^2) + Sk_i}{2(Sq_i - M_i^2)}$$
$$\zeta_i = \frac{\sqrt{\gamma_i^2 + 4(Sq_i - M_i^2)^3} + M_i(3Sq_i - 2M_i^2) + Sk_i}{2(Sq_i - M_i^2)} \tag{A9}$$

ϕ_s is evaluated by substituting p_a from equation (A5) into equation (6), in which derivatives have been numerically solved. As pointed out by Du *et al.* (1994), the linear combination of Gaussian PDFs might not be realistic. A better description of atmospheric turbulence PDF can be given utilising the "maximum missing information" criteria, but the formulation becomes excessively complicated and has not been developed.